ARTICLE IN PRESS

International Journal of Heat and Mass Transfer xxx (2018) xxx–xxx

Contents lists available at ScienceDirect

International Journal of Heat and Mass Transfer

journal homepage: www.elsevier.com/locate/ijhmt

Nano-textured surfaces using hybrid micro- and nano-materials for efficient water cooling

Min-Woo Kim [a,1], Tae Gun Kim [a,1], Hong Seok Jo [a], Jong-Gun Lee [a], Scott C. James [b], Mun Seok Choi [c], Woo Yeong Kim [c], Jae Sin Yang [c], Jeehoon Choi [d,*], Sam S. Yoon [a,*]

[a] School of Mechanical Engineering, Korea University, Seoul 02841, Republic of Korea
[b] Depts. of Geosciences and Mech. Eng., Baylor University, Waco, TX 76798, USA
[c] MS AUTOTECH, 1023 Nogokli, Nanamyun, Gyungju 780-851, Republic of Korea
[d] LG Electronics Inc., Seoul, Republic of Korea

ARTICLE INFO

Article history:
Received 30 October 2017
Received in revised form 28 February 2018
Accepted 28 February 2018
Available online xxxx

Keywords:
Water cooling
Heat removal
Nanotextured surface
Nanomaterials

ABSTRACT

Water cooling heat transfer was enhanced by texturing the heated surface with various micro- and nanomaterials. The increased surface area by texturing facilitated not only enhanced convection, but also turbulent mixing, which increased the effective heat-transfer coefficient. A heated copper substrate was textured with electroplated copper oxide, sprayed silver nanowire, or sprayed copper micro-particles. Sprayed micro-particles were subsequently nano-textured by sand blasting with kanthal (Mo_2Si) nanoparticles. Because of the extremely high hardness of kanthal, sand blasting dimpled the surface to increase the total surface area. Optimal texturing was identified for each material. Hybrid cases combining two different texturing materials were also investigated. All cases were quantitatively compared and that with the highest effective heat transfer was identified. Texturing materials were characterized by scanning electron microscopy and X-ray diffraction. The coating methods are simple, rapid, and scalable and may be cost-effective texturing schemes for various electronics cooling applications.

1. Introduction

Artificial intelligence, the internet of things, big data, cyber-physical systems, and advances in hardware, described as emerging technologies of the fourth industrial revolution, have been combined with web connectivity to impact all disciplines, economies, and industries [1]. These technologies are often based on cloud computing, which is internet- and sever-facilitated computing technology where shared resources, software, and information are provided. Most cloud-computing infrastructures offer services delivered through server-routed data centers. These centers use computing hardware and software products that are specifically designed to deliver cloud services including multi-core semiconductor processors and cloud-specific operating systems. Importantly, advances in high-performance servers hinge on stringent thermal management. Semiconductor chips can require up to 150 W of heat dissipation and cooling solutions are now becoming a limiting factor in technology development. The normal operating temperature of a central processing unit (CPU), graphic processing unit (GPU), and other chips is generally below 70 °C and the reliability of these chips decreases by 10% for each 2 °C increase above this normal operating temperature [2]. To maintain reliability, there is an obvious need for rapid heat removal from CPUs and other chips.

Active air-cooling technology consisting of finned heat sinks combined with fans that transfer heat to outside of the server enclosure. However, air cooling has significant energy demands itself. The total amount of heat transferred from servers into the data center increases the demand on computer room air conditioning (CRAC). Power consumption by data centers constitutes over 0.5% of global power use [3] with power consumption by the CRAC accounting for about 30% of this energy consumption [4–6]. Miniature loop heat pipe systems were introduced to improve air cooling, but have failed widespread commercialization because their complicated fabrication and integration lead to high costs [7–9]. Without technical advances, the CRAC will not be able to economically satisfy the thermal management requirements for servers of the future.

Recently, water cooling has been highlighted as a viable approach for thermal management of data-center severs, although disadvantages include coolant leaks, corrosion fouling, the

* Corresponding authors.
E-mail addresses: choijeehoon@gmail.com (J. Choi), skyoon@korea.ac.kr (S.S. Yoon).
[1] These authors have equally contributed.

https://doi.org/10.1016/j.ijheatmasstransfer.2018.02.120

significant weight of the systems, and the required pumping power [10–14]. Because water has a much higher thermal conductivity, heat capacity, and heat-transfer coefficient than air, the heat dissipation rate using water is much higher than that for air. Heat sinks (called cold plates) on the server enclosure are cooled by circulating water so that a large amount of heat can be directly transferred away from the chips through flexible tubes so that the process is much less influenced by the ambient temperature inside the enclosure [10]. Another advantage is that water cooling is not limited to a single component, but can be set up to cool CPU, GPU, and other components simultaneously within the same system [10,15]. Overall, water cooling provides an efficient solution for the thermal management of data-center servers.

To enhance the capability of the heat sink, researchers have suggested increasing the surface area in contact with water, improving mixing to enhance convective heat transfer, and using micro-scale finned structures [16–20]. However, increasing surface area runs counter to the miniaturization trend while the confined spaces of sever-rack mounts increase pressure drop and associated power consumption. Moreover, the costs of complicated fabrication and integration of finned structures can be prohibitive. Therefore, rapid, simple, and scalable texturing methods at the micro- and nano-scale are desired. At the same time, their micro- and nano-scale structures must not hinder coolant flow through increased capillary pressures. This is important not only to minimize coolant pressure drop, but also so that a continuous supply of coolant can carry heat away from the server.

Researchers have used nano-textured surfaces (copper-plated nanofibers, graphene oxide flakes, and silver nanowires) to enhance heat-transfer rates [21]. These nano-textured surfaces yield large heat-transfer areas even within confined spaces while enhancing the turbulent mixing of the fluid to increase the heat-transfer coefficient. Silver nanowires have shown the most promise. To successfully deploy such a nano-textured surface on the heat sink for servers, however, it is necessary to efficiently dissipate the chip-produced heat and to ensure that components can be easily manufactured in an industrial setting. Therefore, this paper reviews how texturing with silver nanowires can satisfy the cooling requirements in a fashion that is easily adopted.

Herein, we compared the water-cooling performance of various textured surfaces fabricated by supersonic cold spraying (CS), electroplating (EP), and sand blasting. Metals, such as copper and silver with micro- and nano-scale architecture were deposited and their cooling performances were systematically evaluated and compared. The best coating conditions were identified.

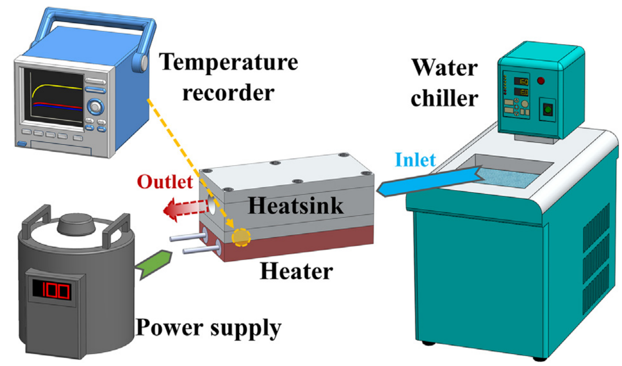

Fig. 1. Schematic of the water-cooling system. Cold water was supplied by the water chiller. The heatsink receives heat from the power supply and water was heated and recycled back to the chiller.

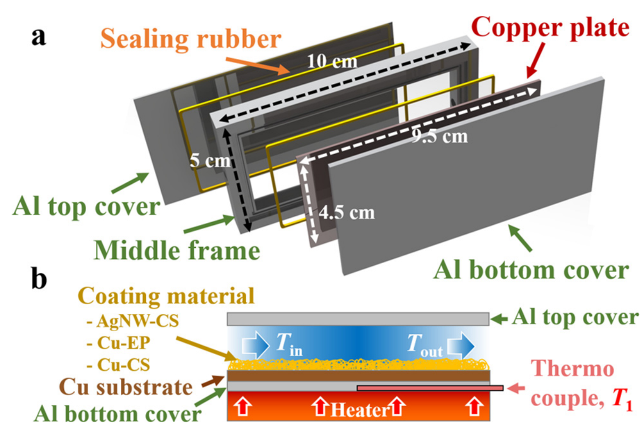

Fig. 2. Detailed schematics of the cooling test module. (a) Assembly of the heat sink. (b) The heat sink attached to the heater. Water entered the heat sink from the left and exited to right.

2. Experimental setup

2.1. Water cooling system

The experimental setup of the water-cooling system is shown in Fig. 1. The water-cooling experimental setup consists of the water chiller (Lab. Companion, RW-0525G), heat sink, temperature recorder (MV-1000, YOKOGAWA, Japan), and power supply. The water chiller supplies cold water at 7 ± 0.5 °C to the heat sink. Warm water returns to the water chiller to cool.

As shown in Fig. 2a, the heat sink consisted of top and bottom covers (aluminum with dimensions of 10 × 5 × 0.5 cm^3), sealing rubber, the middle frame, and the copper-plate substrate (9.5 × 4.5 × 0.7 cm^3) which was textured with micro- and nano-materials. The sealing rubber prevented water leaks. Fig. 2b illustrates the overall heat-transfer scenario through the heatsink. Power was supplied to the heater and its temperature measured at T_1. It should be noted that the substrate surface temperature (T_s) was slightly less than T_1 because heat flowed through the copper medium by conduction, which was quantified using Fourier's Law. Flow rates of 4, 8, and 16 g/s were quantified by measuring volumetric flow over by time. Temperature was measured at the three locations indicated in Fig. 2b: the cold water supplied at the inlet (T_{in}), heated water at the outlet (T_{out}), and the heater temperature, T_1, which was not the same as the substrate temperature, T_s, which was calculated using T_1 with Fourier's Law. T-type thermocouples (probe size of Ø 1.0 × 150 mm) with an accuracy of ±0.1 °C were used.

2.2. Cold sprayed (CS) AgNW and Cu

Silver nanowires (AgNW, Aiden Co., 0.15 wt%) were dispersed in isopropyl alcohol (IPA), average dimensions were 20 nm thick and 15 μm long. A magnetic stirrer maintained a homogeneous suspension of AgNWs, which were aged for 1 h. The AgNW-IPA solution was supersonically sprayed to attach AgNWs onto the copper substrate [21,22]. The supersonic cold spray (CS) setup consisted of a nozzle flowing compressed air over an atomizer to disperse AgNWs from the IPA solution onto the copper substrate. IPA evaporated quickly leaving only AgNWs deposited on the substrate.

The CS system compressed, heated, and accelerated air through a Laval nozzle (operated at conditions listed in Table 1) into which a particle feeder (Praxair 1264i, USA) entrained copper particles to deliver them to the substrate. Variously thick layers of copper particles, which were flattened upon impact, were developed.

Please cite this article in press as: M.-W. Kim et al., Nano-textured surfaces using hybrid micro- and nano-materials for efficient water cooling, Int. J. Heat Mass Transfer (2018), https://doi.org/10.1016/j.ijheatmasstransfer.2018.02.120

Table 1
Operating conditions for CS.

Items	AgNW	Cu particle
Pressure [bar]	4	4
Gas preheating temperature [°C]	550	550
Traverse speed [mm/s]	30	30
Spray distance [mm]	30	30
Powder feed rate [g/min]	–	3

Table 2
Operating conditions for EP.

Items	Conditions
Applied voltage [V]	3
Electrode size [cm × cm]	2.5 × 2.5 (ITO glass) 10 × 5 (copper foil)
Distance between electrodes [cm]	3
Electroplating time [s]	3, 5, 15, 30

2.3. Electroplated (EP) Cu

Another set of textured surfaces was prepared by EP. The copper EP solution included 80 g of copper sulfate (Sigma-Aldrich), 25 g of sulfuric acid (Matsunoen Chemicals), 2.5 g of hydrochloric acid (Sigma-Aldrich), and 50 g of formaldehyde (Sigma-Aldrich) mixed in 500 mL of distilled water. This EP solution was stirred for 1 h at room temperate to obtain a homogeneous solution.

Copper ions in solution were de-oxidized and pure copper layers were formed on the substrate by EP at 3 V using a DC power supply (E3664A, Agilent Technologies) operating at conditions listed in Table 2. EP samples were rinsed with distilled water and dried under an air gun. The EP surface showed visible oxidation when exposed to air.

3. Results and discussion

3.1. Surface morphology

Fig. 3 shows schematics of the three textured surfaces studied. The length scales of the textured surfaces were quite different from one another. For example, for CS AgNWs, the texturing materials had dimensions of 20–30 nm while CS Cu particles flattened into staggered disks were about 1.5 cm. A total of 11 disks were patterned on a copper substrate. EP Cu particles were on the order of a micron.

Fig. 4 shows SEM images of AgNWs coated on the copper substrate. The number of spray passes across the substrate were N = 1, 4, and 8, each increasing the thickness of the AgNW layer. AgNWs were strongly attached onto the substrate because high-speed impact promoted adhesion. When $N = 1$, the substrate was largely exposed. Upon increasing N, the AgNW thickness increased, eventually covering the substrate and reducing the size of the pores between AgNWs. If pores were too small, the permeability decreased and capillary forces trapped liquid in the pores. Thus the optimal number of sweeps was sought.

The SEM images in the second row of Fig. 4 are EP Cu particles that oxidized to copper oxides (Cu_xO). Layer thicknesses were 0.5, 2.5, and 40 μm for EP times of t_{EP} = 3, 5, and 15 s, respectively. Cross-sectional views for each t_{EP} are shown in the insets. Note the micron-scale granularity.

The SEM images in the third row of Fig. 4 show CS Cu particles flattened upon impact [23–26]. The inset shows the top view of the coated sample. Surface morphology was rough due to overlapping impacts of multiple Cu particles. For the specific region selected, magnified views show multiple layers in cross-section.

Fig. 5a illustrates the additional nano-texturing imparted by sand blasting. The CS Cu coating is further textured through impacts by kanthal ($MoSi_2$) particles that dimpled the surface. While CS is often used to coat substrates with "soft" metals [27–29], CS with kanthal dimpled a surface because these hard particles bounced off upon impact [30,31]. Dimples increased the total surface area as shown in Fig. 5b and c. Each micro-scale granule is a flattened Cu particle. Before sand blasting, the surface was fairly smooth; however, after sand blasting, it was nano-textured with numerous dimples. Kanthal has a hardness of 8500 MPa [32], which is about 25 times harder than copper at 350 MPa [33].

Fig. 6 shows X-ray diffractions of each nano-textured surface. The AgNW coating had peaks at 2θ = 37.66°, 43.32°, 64.44°, and 77.64°, which correspond to the (1 1 1), (2 0 0), (2 2 0), and (3 1 1) planes of the face-centered-cubic lattice of silver (JCPDS No. 03-0931), respectively. The second and third curves are the XRD patterns of the EP Cu and CS Cu particle coatings, respectively. Both curves had the same copper peaks at (1 1 1), (2 0 0), and (2 2 0) planes at 2θ = 43.3°, 50.5°, and 74.1°, respectively. However, the EP Cu coating showed evidence of oxidation at the cuprous oxide (Cu_2O) peak at the (1 1 0) plane at 2θ = 28.3°. Additional oxidation states for cupric oxide (CuO) with peaks at (−1 1 1) and Cu_2O (1 1 1) appeared at 2θ = 35.2° and 36.4°, respectively. During electroplating, Cu_2O formed upon oxidation of $4Cu + O_2 \rightarrow 2Cu_2O$. The EP solution consisted of water and hydrochloric acid, which rapidly transformed Cu into Cu_2O. CuO was also formed during the process. Cu_2O was initially formed but was quickly degraded into CuO upon contact with air. Both Cu_2O and CuO had sharply angled surfaces, which in yielded the textured surface. As a result, both the overall surface area and the water-cooling effect increased [34].

3.2. Heat-transfer enhancement

As described in Fig. 2, cold water at $T_{in} = 7 \pm 0.2$ °C flowed through the heat sink, which was heated to T_1 with warm water exiting through the heat sink outlet, T_{out}. Fig. 7a reveals that it takes about 15 min to reach steady state. Fig. 7a shows the change in the steady-state temperature upon increasing coolant flow rate. Heat flow is estimated as

$$\dot{Q}_{flow} = \dot{m} c_p \Delta T, \tag{1}$$

where $\dot{m}$ is the mass flow rate of water, c_p is the specific heat, and $\Delta T = T_{out} - T_{in}$ is the temperature difference between inlet and outlet. Assuming all supplied heat was lost to the coolant (no heat loss to the environment), the heat removed by the cooling water was estimated using the preceding equation and results are summarized in Table 3. Note that the temperature change across the heat sink (i.e., $\Delta T = T_{out} - T_{in}$) was smaller at higher flow rates because the water residence time in the heat sink was shorter, allowing less time for heat exchange; see Table 4. Nevertheless, the increased mass flow rate (even with decreased ΔT) carried away more heat as shown in Table 3. Increased $\dot{Q}$ for higher flow rates is also consistent with the temperature reductions shown in Fig. 7a.

Fig. 8 illustrates the network of thermal resistance of textured materials over the Cu substrate. T_{Cu} is the temperature at the central position of the Cu substrate, and T_s is the temperature at the surface where the Cu substrate contact with AgNW. T_t is the temperature of the AgNW textured on the Cu substrate. These three temperatures were almost the same, but there was actually thermal resistance between each location. The relationship between each temperature and resistance is illustrated as circuit in Fig. 8. The total thermal resistance was:

$$\sum R_{total} = R_1 + R_2 + R_3, \tag{2}$$

Please cite this article in press as: M.-W. Kim et al., Nano-textured surfaces using hybrid micro- and nano-materials for efficient water cooling, Int. J. Heat Mass Transfer (2018), https://doi.org/10.1016/j.ijheatmasstransfer.2018.02.120

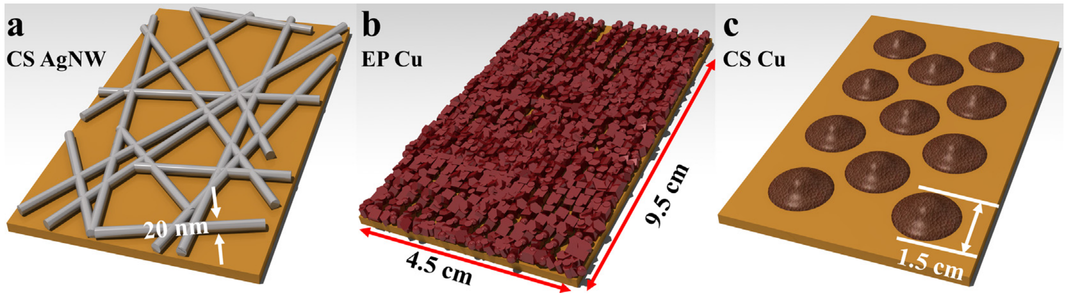

Fig. 3. Schematics of nanotextured surfaces using for CS AgNWs, EP Cu particles, and CS Cu particles on a Cu substrate.

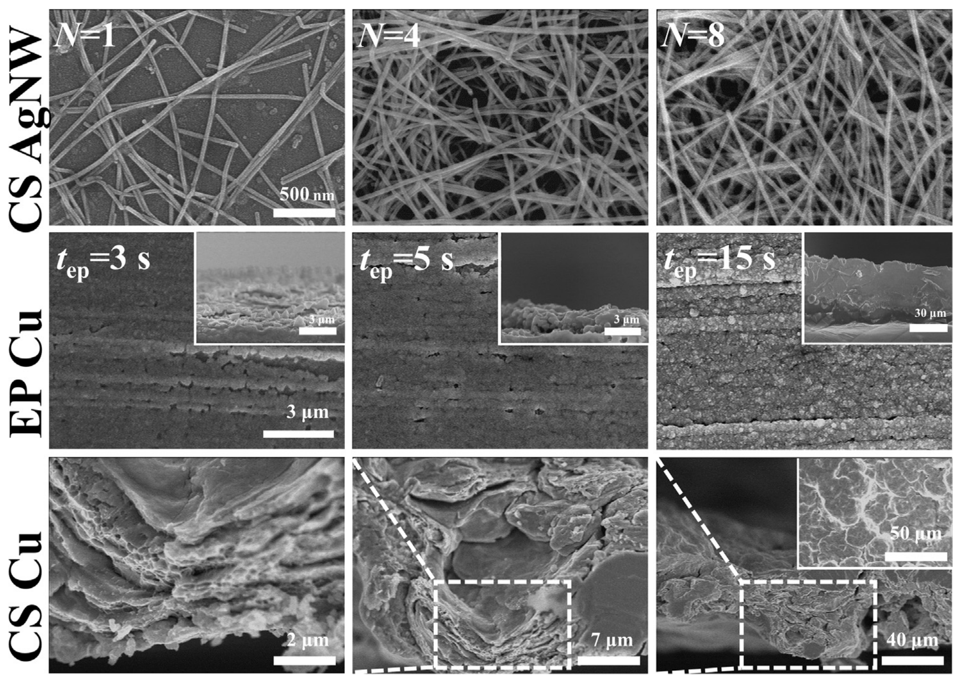

Fig. 4. SEM images of nano-textured substrates. Copper substrate covered with (first row) CS AgNWs, (second row) EP Cu particles, and (third row) CS Cu particles flattened upon high-speed impact.

where R_1 is the thermal resistance of the copper substrate, R_2 is the contact thermal resistance between the substrate and the AgNWs, and R_3 is the thermal resistance due to flow turbulence. For all cases, R_1 was fixed according to the copper substrate; however, R_2 and R_3 change according to the nature of the textured surface and turbulence scale, which can be changed by texturing. R_{total} can be expressed as:

$$R_{total} = \frac{\Delta T}{\dot{Q}}, \quad \dot{Q} = h_{eff} A \Delta T \tag{3}$$

Substituting $Q = h_{eff} \cdot A \cdot \Delta T$ into the preceding equation yields

$$R_{total} = \frac{\Delta T}{h_{eff} A \Delta T} = \frac{1}{h_{eff} A}, \tag{4}$$

where $\Delta T = T_{in} - T_{Cu}$ and A is the projected area of the copper surface (not the textured surface area). For CS AgNW-CS ($N = 1$), meso-scale turbulence promoted turbulent mixing and increased h_{eff}. Upon increasing N, the contact thermal resistance decreased h_{eff}. [21] While R_1 was known, quantitative estimates of R_2 and R_3 were not straightforward and are discussed in the last part of this section.

AgNW coating thickness increased with N (Fig. 7b). More pores formed and water was trapped inside the pores by capillary pressure and did not flow efficiently. This flow resistance increased as the characteristic length-scale decreased because capillary forces increased. For sufficiently high capillary forces, water was trapped inside pores. As a result, an overly thick AgNW layer acted as a thermal barrier and inhibited heat transfer. Increasing N did not necessarily promote heat transfer even though the surface area increased. In fact, $N = 1$ yielded the optimal texturing condition by increasing surface area and turbulent mixing without hindering coolant flow.

Fig. 7c shows the cooling performance for EP Cu for $t_{EP} = 3$, 5, and 15 s. This textured surface reduced T_1 up to $t_{EP} = 5$ as both the surface area (or roughness) and meso-scale turbulence increased to promote mixing and cooling. However, for $t_{EP} = 15$ s, cooling performance was poor. From Fig. 4, the SEM image at $t_{EP} = 15$ s indicates a 40-μm-thick coating with a lot of surface area with greater oxidation. This thick oxidized layer became a barrier to heat transfer due to a decreased thermal conductivity.

In Fig. 7c, temperature trends are similar to those observed for the AgNWs. Upon increasing t_{EP}, both the textured surface area and turbulent mixing increased. However, for the longest t_{EP}, the coating was 40 μm thick with plenty of opportunity for oxidation. From Fig. 4, EP Cu roughness increased with t_{EP} and thus turbulence was enhanced, which decreased R_3. Because h_{eff} decreased for the longest t_{EP}, this indicated that R_2 was the dominant resistance (more important than R_3).

Please cite this article in press as: M.-W. Kim et al., Nano-textured surfaces using hybrid micro- and nano-materials for efficient water cooling, Int. J. Heat Mass Transfer (2018), https://doi.org/10.1016/j.ijheatmasstransfer.2018.02.120

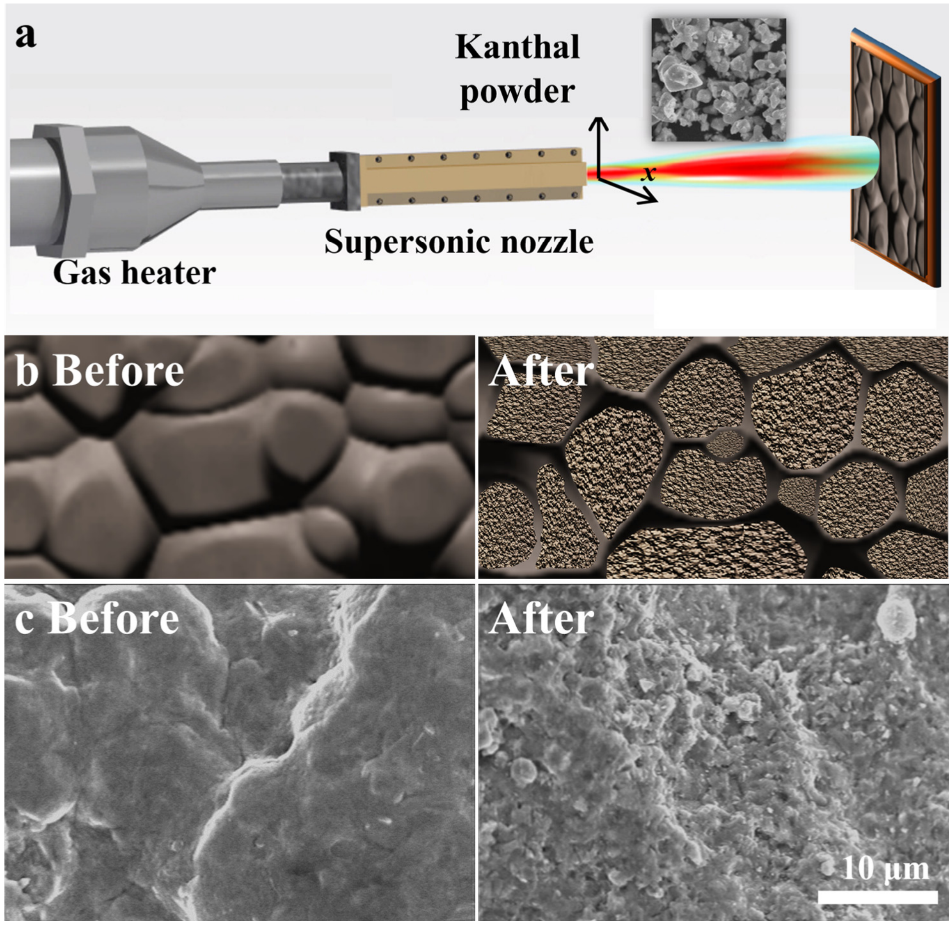

Fig. 5. (a) Supersonic CS sand blasting with kanthal (Mo_2Si) textured the Cu surface and increased its surface area. (b) Artistic illustration of the CS Cu particle coating before and after sand blasting. (c) Actual SEM images before and after sand blasting.

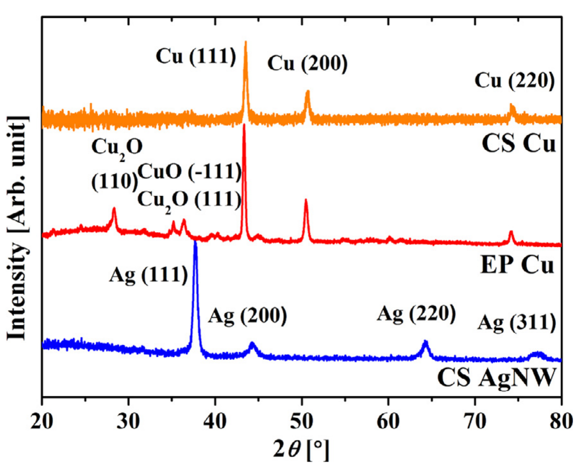

Fig. 6. X-ray diffraction pattern of CS AgNW, CS Cu particles, and EP Cu particles.

So far, $N = 1$ for CS AgnWs, $t_{EP} = 5$ s for EP Cu, and $t_{CS} = 2$ s for CS Cu have been identified as optimal (lowest T_1). Fig. 9 shows T_1 for hybrid cases combining two of the CS, EP, and sand-blasting coating methods. For example, CS Cu coating textured (or sand blasted) with kanthal is identified as "CS Cu + blasting." The other hybrid cases follow similar definitions in Fig. 9.

In Fig. 9, the CS Cu coating textured with sand blasting yielded the lowest $T_1 = 14$ °C. This was a remarkable temperature reduction ($\Delta T = 8$ °C) compared to the uncoated results with $T_1 = 22$ °C. Clearly, additional texturing by sand blasting increased h_{eff} as a result of increased surface area and meso-scale turbulence generated over the dimples.

CS Cu ($t_{CS} = 2$ s) with sand blasting yielded the lowest temperature of $T_1 = 14$ °C. When the pure CS Cu ($t_{CS} = 2$ s) was coated with AgNWs ($N = 1$), the temperature increased to $T_1 = 18.5$ °C; the hybrid approach was not helpful due to the incompatible interface between these different materials. For the same reason, combining EP Cu with CS AgNW increased T_1. In most cases, the hybrid approach of combining two different materials did not improve cooling.

From Fig. 9, EP had the highest T_1 of all texturing methods. Among the hybrid cases, EP Cu + CS AgNW was poorest because of poor thermal compatibility. Note that all texturing outperformed uncoated surfaces.

To quantitatively estimate cooling, h_{eff} was calculated using Newton's Law of Cooling:

$$\dot{Q}_{conv} = h_{eff}A(T_s - T_{in}). \tag{5}$$

Although it was surface area that was changed by nano-texturing, it was not possible to accurately measure its increase. Instead, projected area of the exposed substrate was fixed. Because the same amount of heat must be conducted through the Cu substrate, Fourier's Law of Conduction states:

Please cite this article in press as: M.-W. Kim et al., Nano-textured surfaces using hybrid micro- and nano-materials for efficient water cooling, Int. J. Heat Mass Transfer (2018), https://doi.org/10.1016/j.ijheatmasstransfer.2018.02.120

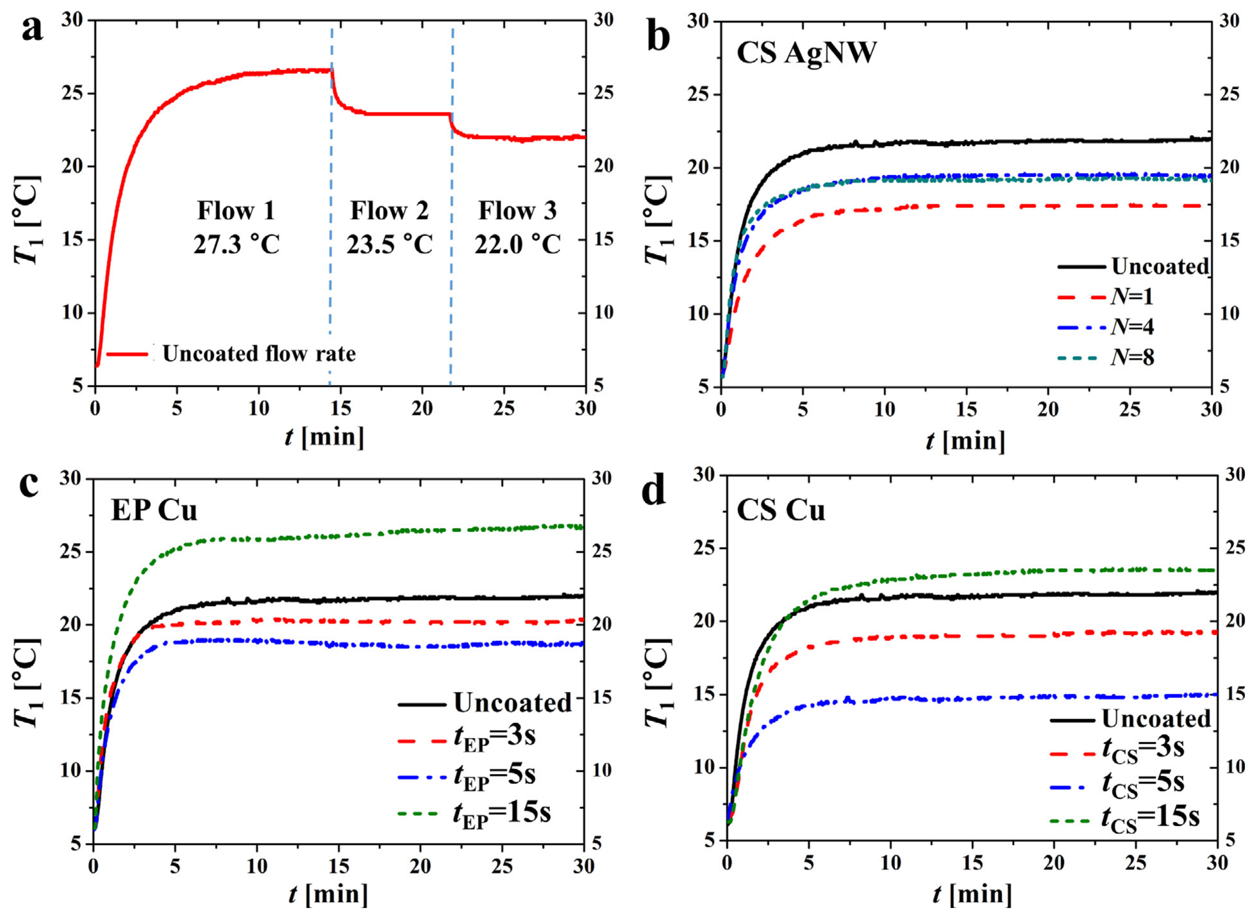

Fig. 7. Steady-state temperatures (T_1) of the heater for each textured surface. (a) Effect of water flow rate. (b) Effect of AgNW coating thickness (N). (c) Effect of t_{EP}. (d) Effect of t_{CS}.

Table 3
The heat removal rate for varied flow rates.

Flow rate	Flow [g/s]	$\dot{Q}$ [J/s]
Flow 1	4	12
Flow 2	8	27
Flow 3	16	68

Table 4
Effective heat-transfer coefficient for the variously textured surfaces.

Case		$\triangle T$ [°C]	h_{eff} [W/m^2 K]
Uncoated Cu substrate	Flow 1	2.0	386
	Flow 2	1.4	663
	Flow 3	1.0	1053
EP Cu (t_{EP} = 5 s)	Flow 3	1.7	2281
CS AgNWs (N = 1)		1.7	2562
CS Cu (t_{CS} = 2 s)		1.7	3217
EP Cu (t_{EP} = 5 s) + AgNW (N = 1)		1.6	1864
CS Cu (t_{CS} = 2 s) + AgNW (N = 1)		1.7	2320
CS Cu (t_{CS} = 2 s) + blasting		1.7	3782

$$\dot{Q}_{\text{cond}} = \frac{kA}{\Delta x}(T_s - T_1), \tag{6}$$

which can be rearranged as:

$$T_s = T_1 + \dot{Q}_{\text{cond}}\frac{\Delta x}{kA}, \tag{7}$$

where k is the thermal conductivity and Δx is the thickness of the copper substrate. The amount of heat removed by the cooling water

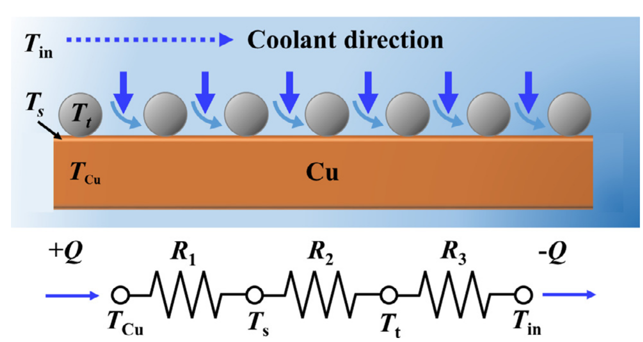

Fig. 8. Schematic of the thermal-resistance network of the textured material.

was approximated by (1), which was equivalent to the convective cooling of (5). This allows the approximation:

$$h_{\text{eff}} = \frac{\dot{Q}_{\text{conv}}}{A(T_s - T_{\text{in}})} \approx \frac{\dot{Q}_{\text{flow}}}{A(T_s - T_{\text{in}})}. \tag{8}$$

Likewise, $\dot{Q}_{\text{cond}}$ is equal to $\dot{Q}_{\text{flow}}$, which yields:

$$T_s = \frac{\frac{k}{\Delta x}T_1 + h_{\text{eff}}T_{\text{in}}}{h_{\text{eff}} + \frac{k}{\Delta x}}. \tag{9}$$

Here, T_s can be estimated because all of the variables on the right hand side are known.

In a similar fashion, (9) can be substituted into (8) to yield

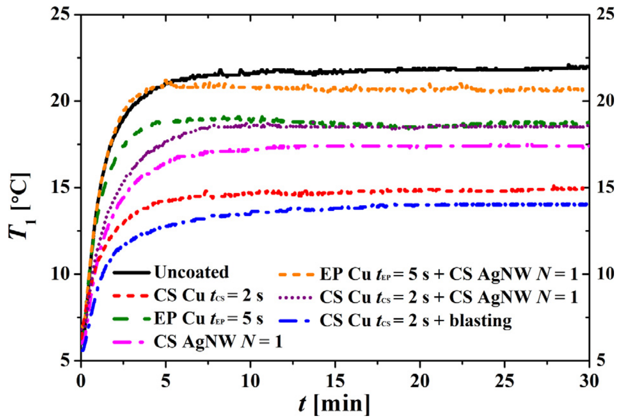

Fig. 9. Cooling effects of nano-textured surfaces.

$$h_{\text{eff}} = \frac{1}{\frac{AT_1}{\dot{Q}_{\text{flow}}} + \frac{\Delta x}{k} - \frac{AT_{\text{in}}}{\dot{Q}_{\text{flow}}}}. \tag{10}$$

For these experiments, $A = 0.095 \times 0.045\ \text{m}^2$ and $T_{\text{in}} = 7\ °\text{C}$. The copper substrate thickness was $\Delta x = 2$ mm.

Table 4 compares h_{eff} across experiments. Flows 1, 2, and 3 indicate the varied flow rates over an uncoated substrate. h_{eff} increased with flow rate according to (1). CS Cu had the highest h_{eff} among single-material coatings. For the hybrid experiments, CS Cu + AgNW outperformed EP Cu + AgNWs. Sand blasted CS Cu had the highest h_{eff} because of the increased surface area of the dimples.

4. Conclusion

Experiments revealed that textured surfaces increased cooling performance through increased surface area and turbulent mixing. However, excessive texturing increased thermal resistance and an optimal was determined for each material. Of all textured surfaces CS Cu exhibited the highest h_{eff}. A simple heat transfer analysis balanced the heat supplied to the substrate with the heat removed by the water so that Newton's Law of Cooling could be used to estimate h_{eff}. These texturing methods are appropriate for electronics cooling applications because of their simplicity and scalability.

Conflict of interest

The authors declare that there is no conflict of interest.

Acknowledgement

This research was primarily supported by MS AUTOTECH. This research was supported by the Technology Development Program to Solve Climate Changes of the National Research Foundation (NRF) funded by the Ministry of Science, ICT & Future Planning (NRF-2016M1A2A2936760), NRF-2013R1A5A1073861, and NRF-2017R1A2B4005639. The research was also supported by the National Research Council of Science & Technology (NST) grant by the Korea government (MSIP) (No. CRC-16-02-KICT).

Appendix A. Supplementary material

Supplementary data associated with this article can be found, in the online version, at https://doi.org/10.1016/j.ijheatmasstransfer.2018.02.120.

References

[1] K. Schwab, The Fourth Industrial Revolution, Penguin, UK, 2017.
[2] A. Bar-Cohen, M. Iyengar, Design and optimization of air-cooled heat sinks for sustainable development, IEEE Trans. Compon. Pack. Technol. 25 (4) (2002) 584–591.
[3] D. Hallett, C. Paunon, Control strategies for data centers-trends around the globe, ASHRAE Trans. 120 (1) (2014).
[4] J.G. Koomey, Estimating total power consumption by servers in the US and the world, February, 2007.
[5] A.D. Series, Best Practices for DataCom Facility Energy Efficiency, Altanta, 2009.
[6] K. Kant, Data center evolution: a tutorial on state of the art, issues, and challenges, Comput. Netw. 53 (17) (2009) 2939–2965.
[7] Y.F. Maydanik, S.V. Vershinin, V.G. Pastukhov, S.S. Fried, Loop heat pipes for cooling systems of servers, IEEE Trans. Compon. Packag. Technol. 33 (2) (2010) 416–423.
[8] J. Ku, H. Nagano, J. Perez, P. Rogers, Thermal performance of a low-cost loop heat pipe, in: International Heat Transfer Conference 13, Begel House Inc., 2006.
[9] J. Choi, B. Sung, C. Kim, D.-A. Borca-Tasciuc, Interface engineering to enhance thermal contact conductance of evaporators in miniature loop heat pipe systems, Appl. Therm. Eng. 60 (1) (2013) 371–378.
[10] T. Chainer, Economizer Based Data Center Liquid Cooling with Advanced Metal Interfaces, IBM, 2012.
[11] M.J. Ellsworth, G.F. Goth, R.J. Zoodsma, A. Arvelo, L.A. Campbell, W.J. Anderl, An overview of the IBM power 775 supercomputer water cooling system, J. Electron. Packag. 134 (2) (2012) 020906.
[12] K. Ebrahimi, G.F. Jones, A.S. Fleischer, A review of data center cooling technology, operating conditions and the corresponding low-grade waste heat recovery opportunities, Renew. Sustain. Energy Rev. 31 (2014) 622–638.
[13] T. Gao, M. David, J. Geer, R. Schmidt, B. Sammakia, Experimental and numerical dynamic investigation of an energy efficient liquid cooled chiller-less data center test facility, Energy Build. 91 (2015) 83–96.
[14] C. Conficoni, A. Bartolini, A. Tilli, G. Tecchiolli, L. Benini, Energy-aware cooling for hot-water cooled supercomputers, in: Proceedings of the 2015 Design, Automation & Test in Europe Conference & Exhibition, EDA Consortium, 2015, pp. 1353–1358.
[15] S. Kang, D. Miller, J. Cennamo, Closed loop liquid cooling for high performance computer systems, in: ASME 2007 InterPACK Conference collocated with the ASME/JSME 2007 Thermal Engineering Heat Transfer Summer Conference, American Society of Mechanical Engineers, 2007, pp. 509–515.
[16] W. Qu, I. Mudawar, Experimental and numerical study of pressure drop and heat transfer in a single-phase micro-channel heat sink, Int. J. Heat Mass Transf. 45 (12) (2002) 2549–2565.
[17] H. Zhang, D. Pinjala, T. Wong, K. Toh, Y. Joshi, Single-phase liquid cooled microchannel heat sink for electronic packages, Appl. Therm. Eng. 25 (10) (2005) 1472–1487.
[18] J. Li, G. Peterson, 3-Dimensional numerical optimization of silicon-based high performance parallel microchannel heat sink with liquid flow, Int. J. Heat Mass Transf. 50 (15) (2007) 2895–2904.
[19] S. Ndao, Y. Peles, M.K. Jensen, Multi-objective thermal design optimization and comparative analysis of electronics cooling technologies, Int. J. Heat Mass Transf. 52 (19) (2009) 4317–4326.
[20] L. Gong, J. Zhao, S. Huang, Numerical study on layout of micro-channel heat sink for thermal management of electronic devices, Appl. Therm. Eng. 88 (2015) 480–490.
[21] H. Yoon, M.-W. Kim, H. Kim, D.-Y. Kim, S. An, J.-G. Lee, B.N. Joshi, H.S. Jo, J. Choi, S.S. Al-Deyab, Efficient heat removal via thorny devil nanofiber, silver nanowire, and graphene nanotextured surfaces, Int. J. Heat Mass Transf. 101 (2016) 198–204.
[22] J.-G. Lee, J.-H. Lee, S. An, D.-Y. Kim, T.-G. Kim, S.S. Al-Deyab, A.L. Yarin, S.S. Yoon, Highly flexible, stretchable, wearable, patternable and transparent heaters on complex 3D surfaces formed from supersonically sprayed silver nanowires, J. Mater. Chem. A 5 (2017) 6677–6685.
[23] J.-G. Lee, J.-H. Lee, S. An, J.Y. Yoon, J.-W. Choi, M.G. Kang, J.I. Lee, H.-E. Song, S.S. Al-Deyab, S.C. James, Effects of impact conditions on the electrical and mechanical properties of supersonic cold sprayed Cu–Ni electrodes, J. Alloys Compd. 695 (2017) 3714–3721.
[24] J.-J. Park, J.-G. Lee, S.C. James, S.S. Al-Deyab, S. Ahn, S.S. Yoon, Thin-film metallization of $CuInGaSe_2$ nanoparticles by supersonic kinetic spraying, Comput. Mater. Sci. 101 (2015) 66–76.
[25] J.-G. Lee, D.-Y. Kim, B. Kang, D. Kim, S.S. Al-Deyab, S.C. James, S.S. Yoon, Thin film metallization by supersonic spraying of copper and nickel nanoparticles on a silicon substrate, Comput. Mater. Sci. 108 (2015) 114–120.
[26] J.-G. Lee, D.-Y. Kim, B. Kang, D. Kim, H.-E. Song, J. Kim, W. Jung, D. Lee, S.S. Al-Deyab, S.C. James, Nickel–copper hybrid electrodes self-adhered onto a silicon wafer by supersonic cold-spray, Acta Mater. 93 (2015) 156–163.
[27] R. Dykhuizen, M. Smith, D. Gilmore, R. Neiser, X. Jiang, S. Sampath, Impact of high velocity cold spray particles, J. Therm. Spray Technol. 8 (4) (1999) 559–564.
[28] C.-J. Li, H.-T. Wang, Q. Zhang, G.-J. Yang, W.-Y. Li, H. Liao, Influence of spray materials and their surface oxidation on the critical velocity in cold spraying, J. Therm. Spray Technol. 19 (1–2) (2010) 95–101.
[29] P.C. King, M. Jahedi, Relationship between particle size and deformation in the cold spray process, Appl. Surf. Sci. 256 (6) (2010) 1735–1738.

Please cite this article in press as: M.-W. Kim et al., Nano-textured surfaces using hybrid micro- and nano-materials for efficient water cooling, Int. J. Heat Mass Transfer (2018), https://doi.org/10.1016/j.ijheatmasstransfer.2018.02.120

[30] W.T. McDermott, J.J. Wu, R.C. Ockovic, Apparatus to Clean Solid Surfaces using a Cryogenic Aerosol, Google Patents, 1993.
[31] P. Schott, Method of using An Abrasive Material for Blast Cleaning of Solid Surfaces, Google Patents, 1996.
[32] P. La, Q. Xue, W. Liu, Study of wear resistant $MoSi_2$–SiC composites fabricated by self-propagating high temperature synthesis casting, Intermetallics 11 (6) (2003) 541–550.
[33] G. Samsonov, Mechanical properties of the elements, in: Handbook of the Physicochemical Properties of the Elements, Springer, 1968, pp. 387–446.
[34] M.-W. Kim, H. Yoon, T.Y. Ohm, H.S. Jo, S. An, S.K. Choi, H. Park, S.S. Al-Deyab, B. K. Min, M.T. Swihart, Nanotextured cupric oxide nanofibers coated with atomic layer deposited ZnO-TiO_2 as highly efficient photocathodes, Appl. Catal. B 201 (2017) 479–485.

Please cite this article in press as: M.-W. Kim et al., Nano-textured surfaces using hybrid micro- and nano-materials for efficient water cooling, Int. J. Heat Mass Transfer (2018), https://doi.org/10.1016/j.ijheatmasstransfer.2018.02.120